International Journal for Housing Science and Its Applications
Publish August 10, 2025. Volume 46, Issue 4 Pages 6936-6953

https://doi.org/10.70517/ijhsa464599

Autonomous Parking System for Intelligent Connected Vehicles in Closed Residential Areas: Research on Multi-Sensor Fusion Localization and Path Planning Algorithms

Ke Zhang[1] and Lijun Liu[2,*]
[1] Chongqing Industry Polytechnic College, Chongqing, 401120, China
[2] China Automotive Engineering Research Institute Co., Ltd., Chongqing, 401122, China
Corresponding authors: (e-mail: zhohagle86@126.com).

Abstract Intelligent networked vehicles face parking problems in the process of urbanization, and closed residential areas put forward higher requirements for autonomous parking systems due to the characteristics of narrow space and complex obstacles. Aiming at the autonomous parking problem of intelligent networked vehicles in the narrow parking space of closed residential areas, this paper proposes a path planning algorithm based on multi-sensor fusion localization. The algorithm constructs an environmental data acquisition system containing 12 ultrasonic sensors and 4 high-definition cameras, and establishes a multi-sensor fusion framework with a camera model, an IMU measurement model, and a kinematic model of a wheel tachometer. An improved inverse extension Hybrid A* path planning algorithm is designed, which improves the planning efficiency by interchanging the start point and the target point, so that the algorithm expands the nodes from inside the narrow space to the open space. The simulation experiment results show that the path planning time of the algorithm in different scenarios is within 1.4s, of which the fastest planning time is 0.75s. In the test of different parking space sizes, the minimum required parking space size is 6.821m×2.164m when the vehicle speed is 3km/h, and increases to 7.058m×2.205m at 6km/h. The algorithm successfully realizes safe path planning for vertical and parallel parking scenarios, and the error of the vehicle's intersecting position with the parking space line is controlled within 12 cm. This study provides an effective technical solution for autonomous parking of intelligent connected vehicles in complex residential environments.

Index Terms intelligent connected vehicle, multi-sensor fusion, autonomous parking, path planning, Hybrid A* algorithm, localization

I. Introduction

In the process of urban development, the planning and construction mode of residential area has always been a topic of great concern, among which, closed residential area is a common type, which has a far-reaching impact on the spatial layout of the city, the lifestyle of the residents, and the development of the society [1]-[4]. A closed residential area is a residential area with clear boundaries, usually enclosed by walls or fences, which restricts the free access of outsiders and has perfect property management and supporting facilities inside [5]-[7]. This community model in has a long history and has satisfied people's needs for security, privacy and environmental quality for a certain period of time [8], [9]. However, there are some shortcomings in closed residential areas, especially in the current society of large car ownership, closed residential areas due to the walls and fences make the city's road network become incoherent, which increases the difficulty of parking and reduces the efficiency of the road, and the application of intelligent networked vehicle autonomous parking system can solve this problem [10]-[13].

Intelligent networked cars equipped with advanced on-board sensors, controllers, actuators and other devices, and the integration of modern communication and network technology, can realize the V2X intelligent information exchange and sharing, with complex environment perception, intelligent decision-making, collaborative control and implementation of the functions, can realize safe, comfortable, energy-saving, efficient driving, and ultimately can be a substitute for the operation of people to operate a new generation of cars [14]-[17]. Among the intelligent connected vehicles, autonomous parking is more mature. For example, the autonomous parking system proposed by BenQ Electronics is a set of unmanned parking solutions, which solves the parking restriction problem through the air-suspended whole vehicle [18]-[20]. In terms of autonomous parking systems, Bosch's VoiceParkSystem has developed an intelligent parking technology for drivers, which can tell the system the specific location where they want to park through voice commands and automatically find an empty space to enter, and record the parking process using a car recorder [21]-[24].

The problems of traffic congestion and lack of parking resources in modern cities are becoming increasingly serious, especially in densely populated residential areas, where parking difficulties have become an important factor affecting the quality of life of residents. Closed residential areas bring great challenges to traditional manual parking due to their unique spatial layout characteristics, including narrow passages, complex geometric structures, and dense distribution of parking spaces. Drivers need to complete precise vehicle maneuvering in a limited space, which not only tests driving skills, but also has a high risk of collision. At the same time, frequent reversing and adjustment actions increase the parking time and reduce the efficiency of the parking lot. In this context, the development of intelligent autonomous parking technology provides a new idea to solve this problem. Autonomous parking system can realize automatic parking of vehicles in the case of no intervention through advanced sensor technology and intelligent algorithms, which can not only reduce the burden of drivers, but also significantly improve parking accuracy and efficiency. However, the complex environment of closed residential areas puts forward higher technical requirements for autonomous parking systems, including high-precision environment sensing, accurate vehicle positioning, and optimized path planning capabilities.

Based on the above problems, this study proposes a comprehensive technical solution. First, a multi-sensor fusion localization system is constructed, which integrates information from multiple sensors such as ultrasonic sensors, high-definition cameras, IMUs, and wheel tachometers, to achieve accurate sensing of the vehicle position and the surrounding environment. Then, a complete sensor mathematical model, including camera projection model, IMU error model and vehicle kinematics model, is established to provide a theoretical basis for subsequent data fusion. Then, an improved inverse extended Hybrid A* path planning algorithm is designed for the characteristics of narrow space in closed residential areas, and the planning efficiency and path quality of the algorithm in complex environments are improved by optimizing the search strategy and the design of the cost function. Finally, the effectiveness and robustness of the proposed algorithm in different parking scenarios are verified through simulation experiments to provide technical support for practical applications.

II. Autonomous parking path planning algorithm based on multi-sensor fusion localization

In this chapter, the parking problem is modeled based on the environmental data acquisition system and sensor model, and a path planning algorithm based on multi-sensor fusion localization is proposed with a view to be used in the algorithm design of autonomous parking system for smart networked vehicles in closed residential areas.

II. A.Environmental data acquisition systems

The prerequisite for successful autonomous parking is to be able to correctly perceive the environment around the body, correctly recognize the empty parking space and determine whether the space meets the conditions for autonomous parking. The environmental data acquisition system consists of short-range ultrasonic sensors, long-range ultrasonic sensors and high-definition cameras arranged around the car body, which detects the distance to the surrounding vehicles and other obstacles through the radar and high-definition cameras, and uses the ABS wheel speed sensors to obtain the speed signals to determine the distance of the vehicle, and uses the two parameters to establish the environmental model of the parking space, and determines whether the size of the parking space is appropriate.

Based on the ultrasonic space scanning technology, it can detect the distance between the body and the surrounding obstacles in real time, and then calculate the vehicle driving distance through the ABS wheel speed signal, and resolve the available parking space through the algorithm.

Because the ultrasonic waveform is a sector and a single ultrasonic detection can not identify the orientation of the detected object, so the vehicle speed in the forward driving process due to changes in speed, lateral distance, the echo time will change, APA in the parking process, will track the trajectory and through the real-time 12 sensors to correct the data to realize the automatic parking.

The image data processing process is shown in Figure 1, based on the image characteristics of the spatial scanning technology, through the camera to establish the visual perspective of the ranging model, calculate the distance between the camera and the image feature points in the real space of the corresponding points, and then establish a comprehensive test model to calculate the final parking space length, width and the entry vehicle and parking space relative distance. The fusion scheme is based on ultrasonic radar and AVM fusion technology as the space detection and path planning, body localization, and steering control tracking of the parking space to automatically control the vehicle to park into the parking space.The APA controller is integrated in the AVM panoramic controller. There are six ultrasonic sensors and one HD camera at the front and rear of the vehicle, and one HD camera at each of the left and right rearview mirrors, totaling twelve ultrasonic sensors and four HD camera modules.

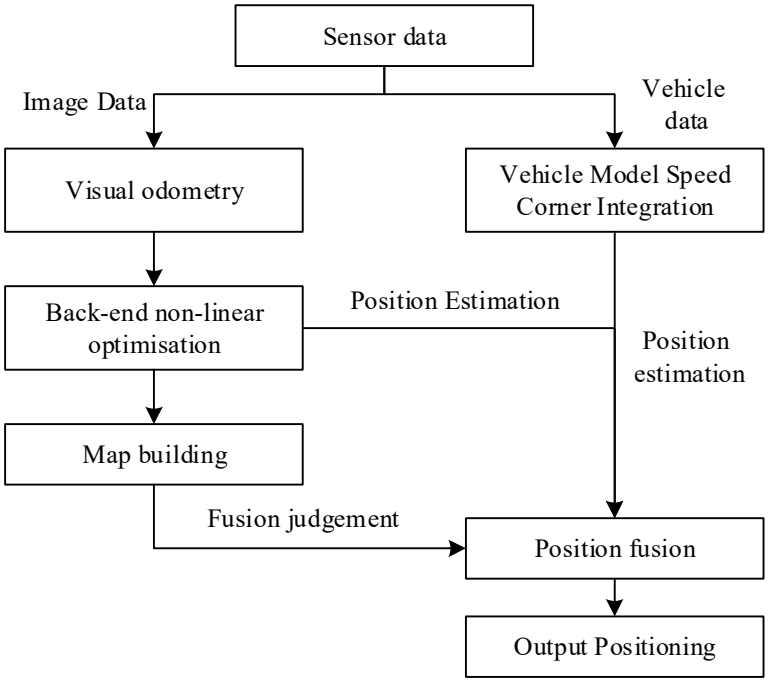

Figure 1: Image data processing flow

II. B.Sensor models

II. B. 1) Camera model

The process by which a camera maps a point in three-dimensional space to a two-dimensional image plane can be modeled as a geometric model, also known as a camera model, which can be interpreted as a combination of a projection model and an aberration model. For the projection model there are pinhole camera model, omnidirectional model and uniform projection model, of which the most widely used is the pinhole camera model, which is an idealized model based on the principle of small hole imaging pan. In this model, a point in the 3D world is projected onto the imaging plane through a virtual “pinhole”. This imaging plane is located on the opposite side of the pinhole and is, in fact, mathematically equivalent to the sensor plane of a camera. Since light is reversed as it passes through the pinhole, the image on the imaging plane is an inverted and reversed version of the real-world scene. In the pinhole camera model, we can describe the relationship between a point in space and its projected point on the imaging plane by the principle of similar triangles. Let a point $P(X,Y,Z)$ in 3D space and its projection point $p(u,v)$ on the imaging plane can be transformed by Equation (1):

$$\begin{aligned} u &= f_x \frac{X}{Z} + c_x \\ v &= f_y \frac{Y}{Z} + c_y \end{aligned} \tag{1}$$

where f_x and f_y are the focal lengths of the camera in the horizontal and vertical directions, respectively, in pixels, and c_x and c_y are the coordinates of the principal points on the imaging plane, i.e., the pixel coordinates of the intersection points of the optical axis and the imaging plane.

In order to enhance the imaging effect of the camera, lens modules are often added to the camera, and because the shape of the lens will produce a change in the propagation path of the light, so that a straight line in the real environment becomes a curve on the imaging plane, this aberration caused by the shape of the lens is known as the radial aberration, which is mainly divided into barrel aberration and cushion-shaped aberration. In practice, the installation plane of the lens and the imaging plane will inevitably have an angular error, so it will cause tangential aberrations. Usually, the Rantan aberration model is used for modeling, considering a point $p(x,y)$ on the normalization plane, which can be represented by polar coordinates (r,θ), the radial aberration is related to r, and the tangential aberration can be regarded as the change of the coordinate point along the tangential direction, so the aberration is described by using a high degree polynomial, that is:

$$\begin{cases} x_{distorted} = x(1+k_1r^2+k_2r^4+k_3r^6) \\ y_{distorted} = y(1+k_1r^2+k_2r^4+k_3r^6) \end{cases} \tag{2}$$

where $[x_{distorted}, y_{distorted}]^T$ are the normalized coordinates of the distorted point. For tangential distortion, it is corrected by p_1, p_2:

$$\begin{cases} x_{distorted} = x+2p_1xy+p_2(r^2+2x^2) \\ y_{distorted} = y+p_1(r^2+2y^2)+2p_2xy \end{cases} \tag{3}$$

From Eqs. (1)~(3), a point $P(X,Y,Z)$ in space is known to be projected to the normalized image plane coordinates $p(x,y)$, and the de-distorted point coordinates are computed in the normalized plane:

$$\begin{cases} x_{distorted} = x(1+k_1r^2+k_2r^4+k_3r^6)+2p_1xy+p_2(r^2+2x^2) \\ y_{distorted} = y(1+k_1r^2+k_2r^4+k_3r^6)+p_1(r^2+2y^2)+2p_2xy \end{cases} \tag{4}$$

By projecting the de-distorted points onto the pixel plane through the in-camera parameters, the projection of a 3D point onto the image plane is realized:

$$\begin{cases} u = f_x x_{distorted} + c_x \\ v = f_y y_{distorted} + c_y \end{cases} \tag{5}$$

II. B. 2) IMU Measurement and Motion Modeling

The IMU consists of three orthogonal-axis accelerometers and gyroscopes with a total of six degrees of freedom, which can measure the acceleration information and angular velocity information of the carrier in three directions, respectively.

When using IMU for attitude estimation, it is often necessary to integrate the measured values against time, and the integration process will introduce cumulative errors, so it is necessary to model the errors of the accelerometers and gyroscopes.The errors of the IMU can be divided into deterministic and random errors, where the deterministic errors include the zero bias, the scale factor, and the non-orthogonality errors, which can be determined by pre-calibration before leaving the factory, and the random errors The random error includes measurement error and zero-bias random wander error, which is not a fixed parameter value, and it is usually assumed that the random error noise obeys a Gaussian distribution.The measurement model of IMU can be expressed by the following equation:

$$\begin{aligned} a^B &= R_W^B\left(a^W - g^W\right)+b_a+n_a \\ \omega^B &= \omega^B + b_\omega + n_\omega \end{aligned} \tag{6}$$

where a^B and ω^B denote the high-frequency measurements of the accelerometer and gyroscope, respectively. a^W denotes the true value of the acceleration of the IMU in the world coordinate system $\{W\}$, and ω^B denotes the true value of the angular velocity of the IMU in the body coordinate system $\{B\}$. R_W^B denotes the rotational transformation from the world coordinate system $\{W\}$ to the intrinsic coordinate system $\{B\}$. b_a and b_ω denote the zero bias of the accelerometer and gyroscope, respectively. n_a and n_ω denote the measurement noise of the accelerometer and gyroscope, respectively.

II. B. 3) Kinematic modeling of the wheel tachometer

Ackermann's motion model is used for general real vehicles, and its motion mechanism includes two core components: the steering mechanism and the differential. The steering mechanism is used to control the steering of the front wheels, and the differential is used to automatically distribute the power output of the motor to the left and right wheels, which can automatically adjust the speed of the two rear wheels according to the steering angle of the steering mechanism.

In order to simplify the motion of the vehicle, the bicycle model is often used to simplify the Ackermann model, in the simplification of the bicycle model needs to assume that the form of vehicle motion is approximated as a planar motion, and the front and rear of the same side of the two tires of the same speed and angle of rotation. The average

deflection angle θ_H of the front wheel and the speed of the rear wheel v_R are known, and in the turning state of the vehicle, the velocity of the center of mass point of the vehicle in the x, y direction and the steering angular velocity are respectively:

$$\begin{aligned} \dot{\psi} &= \frac{v_R \tan\theta_H}{L} \\ \dot{X} &= v_R \cos\psi \\ \dot{Y} &= v_R \sin\psi \end{aligned} \tag{7}$$

II. B. 4) Kinematic modeling of the wheel tachometer

Global Navigation Satellite System (GNSS) is a satellite-based positioning system, and its basic principle is the three-point positioning method, i.e., through the receiver to measure the arrival time of the satellite signal and the satellite ephemeris to determine the signal propagation time, so as to estimate the distance between the GNSS receiver and each satellite, and based on the principle of triangulation to determine the positioning information of the GNSS receiver, but the actual application of GNSS signal propagation distance is very far, during which it will be affected by the atmospheric ionosphere, troposphere, clouds and other natural environment interference, so the positioning error is larger. However, in practice, the GNSS signal propagation distance is very far, during which it will be interfered by the natural environment such as atmospheric ionosphere, troposphere, clouds, etc., and will also be affected by the Doppler effect generated by the satellite's high-speed movement, so the positioning error is larger.

In order to better eliminate the error and improve the positioning accuracy of the GNSS receiver, this system uses RTK technology to improve the positioning accuracy, providing centimeter-level positioning accuracy by using real-time differential corrections between the reference station and the mobile station.The working principle of RTK technology is that, during the measurement process, the GNSS receiver of the mobile station receives the satellite signals and compares them with the same satellite signals received by the reference station. The reference station knows its exact position and estimates the errors in the propagation of the satellite signal. The reference station sends this error information to the mobile receiver, and the mobile uses the differential correction data to correct its own measurements, thus improving the measurement accuracy.

Although RTK technology can provide very high positioning accuracy, in underground parking lot environments or scenes with more serious occlusion, the satellite signal will still be greatly affected and the positioning information cannot be used. Therefore, in order to meet the demand for high-precision and high-robustness positioning, it is necessary to fuse GNSS and other sensors to meet the needs of autonomous parking tasks.

II. C.Modeling the Parking Problem

II. C. 1) Vehicle kinematic modeling

Autonomous operating vehicle speeds do not exceed 15km/h on the parking lot road and 5km/h during parking.Under these non-extreme working conditions of low speed and less transient problems of large acceleration start-stop, the following assumptions can be made:

(1) In the low-speed form, ignoring the side deflection characteristics of the tires, the velocity directions of the front and rear wheels are the steering angle directions of the front and rear corners.

(2) Only the motion of the vehicle on the XOY plane is considered, i.e., the vehicle described in this paper is a moving object on a two-dimensional plane.

(3) The previously mentioned assumption that each of the two front/rear wheels has the same steering angle, so it can be merged into a single tire and simplified to a single vehicle model.

(4) The body and suspension system are rigid.

Under low-speed driving conditions, the vehicle model in autonomous driving can be simplified as a rigid structure moving on a two-dimensional plane, and the origin of the vehicle coordinates at any moment is located at the center of the rear axle, and the coordinate axis is parallel to the body. v denotes the velocity at the center of the rear axle of the vehicle, δ denotes the front wheel angle of rotation, L denotes the distance between the front wheel and the rear wheel, L_f denotes the length of the front overhang, L_r denotes the length of the rear overhang, the width of the vehicle is $2b$, and θ is the angle of the vehicle's body facing to the x-axis of the world coordinate system. If δ remains constant, the vehicle turns in place with a turning radius of R. The rear suspension center of the vehicle is $O_b(x, y)$.

A simple vehicle kinematics can be expressed as:

$$\begin{bmatrix} \dot{x} \\ \dot{y} \\ \dot{\theta} \end{bmatrix} = v * \begin{bmatrix} \cos\theta \\ \sin\theta \\ \frac{\tan\delta}{L} \end{bmatrix} \tag{8}$$

The model can be further represented in a more general form:

$$\dot{\psi} = f(\psi, u) \tag{9}$$

where the state quantity ψ is:

$$\psi = [x, y, \theta]^T \tag{10}$$

The control quantity u is:

$$u = [v, \delta]^T \tag{11}$$

where x is the transverse coordinate of the vehicle rear suspension center, y is the transverse coordinate of the vehicle rear suspension center, θ is the vehicle heading angle, v is the vehicle velocity, and δ is the vehicle front wheel turning angle.

II. C. 2) Parking lot map model

In this paper, a parking lot environment map is created in the Gazebo simulation environment, which is equipped with an intelligent parking system by default, and is able to intelligently identify the number of vacant parking spaces, location coordinates, spatial coordinate information of lanes, and congestion. In order to complete the task of autonomous valet parking, this paper establishes a topological map model and a raster map model for the structured parking lot environment in the simulation.

(1) Topological map of parking lot

Topological map is a relatively more abstract form of map, which represents the indoor environment as a topological structure with nodes and related connecting lines. In a topological map, nodes represent important location points in the environment, such as corners, doors, elevators, staircases, etc., while edges represent the connectivity between nodes, such as corridors. Topological maps simplify map representation by representing key points in the environment and the connections between them. Compared to metric maps, topological maps are usually smaller, and nodes and edges in topological maps can be easily added, deleted, or updated, which makes it relatively easy to maintain and update the map. This level of abstraction helps the robot to plan paths and avoid obstacles.

Based on the functional description of smart parking lots in related literature, this paper agrees on the following rules:

a) The spatial location information of the parking nodes in the topological map has been recorded, and the autonomous parking system can obtain the spatial location of the parking space and the status of the parking space through the node number: idle or occupied.

b) Intersection, drive-in lane, drive-out lane spatial location information has been recorded, the autonomous valet parking system can obtain the spatial extent of the lane, intersection representation and congestion status through the lane number, intersection number.

(2) Parking lot raster map

Since the path planning algorithm used in this paper needs to know the location and contour information of obstacles, this paper establishes a raster map for the parking lot simulation environment. Raster map is a grid-based map representation method, using a two-dimensional matrix to store environmental information, simple storage structure, and fast random access speed. Raster maps can be selected according to the requirements of the application scene with appropriate grid size and map resolution.

In this paper, two raster maps are used: a global static raster map, which stores all the static obstacle information of the entire parking lot. The obstacles in the global static raster map are not inflated, and only the information of whether the grid in the map is occupied by obstacles is retained, which is due to the fact that the global planning algorithm used in the navigation phase of this paper does not need to use the grid surrogate value information of the inflated region. The other is the local dynamic raster map, in this paper the local dynamic raster map is centered on the vehicle rear suspension center point to construct the expansion map, with the movement of the vehicle, the

obstacle information in the local dynamic map will be updated in real time. The local replanning algorithm in this paper will use the raster surrogate value of the inflated map to plan a safe and reliable local path.

II. C. 3) Vehicle collision detection

Vehicles should be guaranteed to be collision-free throughout the autonomous valet parking process, and the establishment of collision constraints is crucial for collision detection. Common collision detection schemes model the vehicle contour as a single-circle model, a double-circle model, and a rectangular model.

Among them, the rectangular model is the model closest to the vehicle contour, which produces the smallest redundant space and allows the vehicle to complete more accurate path planning in a narrow space. The rectangular model has no rotational invariance in the world coordinate system, and the rectangular contour needs to be calculated according to the current state of the vehicle.

The rear suspension center of the vehicle is known to be $O_b(x_r, y_r)$, and let the rectangular vehicle model have the left rear vertex $A(x_a, y_a)$, the right rear vertex $B(x_b, y_b)$, the right front vertex $C(x_c, y_c)$, and the left front vertex $D(x_d, y_d)$. From the geometric relationship, the coordinates of the 4 vertices can be calculated as shown in Eqs. (12) to (15):

$$\begin{bmatrix} x_a \\ y_a \end{bmatrix} = \begin{bmatrix} x_r - L_r\cos\theta + b\cos\theta \\ y_r - L_r\sin\theta - b\sin\theta \end{bmatrix} \tag{12}$$

$$\begin{bmatrix} x_b \\ y_b \end{bmatrix} = \begin{bmatrix} x_r - L_r\cos\theta + b\sin\theta \\ y_r - L_r\sin\theta - b\cos\theta \end{bmatrix} \tag{13}$$

$$\begin{bmatrix} x_c \\ y_c \end{bmatrix} = \begin{bmatrix} x_r + (L + L_r)\cos\theta + b\sin\theta \\ y_r + (L + L_r)\sin\theta - b\cos\theta \end{bmatrix} \tag{14}$$

$$\begin{bmatrix} x_d \\ y_d \end{bmatrix} = \begin{bmatrix} x_r + (L + L_r)\cos L_r - b\sin\theta \\ y_r + (L + L_r)\sin\theta + b\cos\theta \end{bmatrix} \tag{15}$$

where L is the distance from the front suspension center to the rear suspension center of the vehicle, L_r is the length of the rear suspension, and θ is the vehicle heading angle.

Sampling at equal distances on the rectangular contour formed by 4 vertices, determine whether the sampling point is in the obstacle area, if there is a sampling point in the obstacle area, then the collision occurs.

II. D.Autonomous parking path planning algorithm design

In this section, an improved Hybrid A* path planning algorithm [25] for narrow parking spaces in closed residential areas is proposed to improve the efficiency of autonomous parking path planning.

II. D. 1) Consideration Maps and Collision Detection

(1) Rasterized cost map

This paper uses a rasterized cost map to represent the search space for path planning. The cost map stores information about the environment of the space where the vehicle is located, which includes passable areas, obstacle areas, and non-crossable areas. The rasterized cost map used in this paper consists of a series of two-dimensional rasters, where each raster is assigned a value in the interval [0,1] to represent the cost consumed by the vehicle when it passes through the raster. Whether a vehicle can pass through a grid is determined by the state of the grid, which is set to three states, “Occupied”, “Free” and “Unknown”. Unknown”. Among them, the “Occupied” state can be divided into two kinds, which are “obstacle” and “inflated area”. What state the raster is in needs to be determined by the two parameters occupied threshold and passable threshold.

(2) Expansive collision detection

In this paper, the expansion collision detection algorithm is used to determine whether the vehicle position is in a collision state, the workflow of the algorithm is as follows:

Step 1: Calculate the expansion radius according to the vehicle parameters. The initial expansion radius is the radius of the smallest set of overlapping circles required to completely encircle the vehicle, and the centers of the overlapping circles are distributed on the longitudinal axis of the vehicle. The size of the expansion radius can be reduced by increasing the number of overlapping circles, and a smaller expansion radius is conducive to improving the accuracy of collision detection.

Step 2: According to the size of the expansion radius the grid of the area where the obstacle is located is expanded outward. If the expansion radius is not equal to an integer multiple of the grid edge length, then the expansion radius should be rounded up to an integer multiple of the grid edge length.

Step 3: The expanded grids form an expanded region of the obstacle, and all grids in the expanded region are marked as occupied, and the vehicle is not allowed to pass through the grids.

Step 4: Detect whether the center of the overlapping circle on the longitudinal axis of the vehicle is located in the grids in the inflated region. There are three kinds of detection results as follows:

a) A collision occurs: if the center of the circle is located inside the grid in the expansion region, the vehicle is in a collision.

b) No collision: if the center of the circle is not located inside the grid in the inflated region and the surrogate value of the grid in which the center of the circle is located is less than the passable threshold, the vehicle does not have a collision.

c) Unable to judge: If the center of the circle is not located inside the grid in the expansion area, but the surrogate value of the grid where the center of the circle is located is greater than the passable threshold, it is not possible to judge whether the vehicle has been in a collision or not. In the case where it is impossible to judge the detection result, the vehicle is not allowed to pass in that grid.

II. D. 2) Hybrid A⋆ Path Planning Algorithm

(1) Hybrid state search space characterization

The search space of Hybrid A⋆ is used to store the path node information of both continuous and discrete states, and the continuous and discrete states together form a hybrid state. In the hybrid state search space, both the continuous state and the discrete state contain the position information and attitude information of the vehicle. The continuous state (x, y, θ) is used to ensure that the path generated by Hybrid A⋆ is a smooth curve. Where (x, y) is the position of the vehicle's rear axle center and θ is the vehicle traverse angle. The continuous state is discretized to ensure that the raster of the cost map can be searched efficiently. The discrete states $(\tilde{x}, \tilde{y}, \tilde{\theta})$ are obtained by converting the continuous states:

$$\tilde{x} = \frac{x - O_x}{\sigma} \tag{16}$$

$$\tilde{y} = \frac{y - O_y}{\sigma} \tag{17}$$

$$\tilde{\theta} = \frac{\theta}{\sigma_\theta} \tag{18}$$

where (O_x, O_y) is the coordinate origin position of the cost map, σ is the side length of the square raster, and σ_θ is the discretized unit transverse pendulum angle.

(2) Node Expansion Conditions

The node expansion of Hybrid A⋆ is realized by expanding the step size. The following conditions need to be satisfied for the expansion step:

a) When expanding a node, the number of expansion steps n_l in a single expansion is positively odd, and a single expansion step of length l must span out of the current grid, with the following conditions:

$$l > \sqrt{2}\sigma \tag{19}$$

b) The curvature of the extended step is limited by the maximum turn angle of the front wheels of the vehicle $\delta_{\max}$, as specified in the condition:

$$-\delta_{\max} \le \delta \le \delta_{\max} \tag{20}$$

c) The amount of change in the front wheel angle of the vehicle $\Delta\delta$ is an integer multiple of the discretized unit transverse pendulum angle σ_θ, with specific conditions:

$$\Delta\delta = k\sigma_\theta, k \in Z \tag{21}$$

(3) Cost function design

The path is connected by a series of optimal nodes. In the process of searching the path nodes, the optimal node n^* is selected by the calculation of the cost function $f(n)$, and the alternative node with the smallest surrogate value is selected as the optimal node. The cost function $f(n)$ is calculated by the formula:

$$f(n) = \lambda_n g(n) + h(n) + c_n \tag{22}$$

Where: n is the current node. $g(n)$ is the cumulative cost, denoting the cost from the starting node to the current node, which is calculated as:

$$g(n) = \sum_{i=1}^{n} l_i \tag{23}$$

The λ_n denotes the penalty coefficient of node expansion direction. In the process of planning paths, the forward and backward expansion tendency of a node can be controlled by adjusting the penalty coefficient λ_n of the node's expansion direction, which is calculated by the formula:

$$\lambda_n = \begin{cases} c_{forward} & \text{Expansion step is forward} \\ c_{reverse} & \text{Extended step is backward} \end{cases} \tag{24}$$

c_n is the penalty coefficient for the occurrence of switching in the node extension direction. In the process of planning paths, the frequency of switching between the front and back extension directions of a node can be controlled by adjusting the penalty coefficient c_n for the occurrence of switching in the extension direction of the node, which is calculated by the formula:

$$c_n = \begin{cases} 0 & \text{Expansion step direction is unchanged} \\ c_{direction} & \text{Extended step direction change} \end{cases} \tag{25}$$

$h(n)$ is the heuristic function, also known as the predicted cost, which represents the cost from the current node to the target node. The heuristic function can guide the expansion direction of the node so that the node expands towards the target node, thus speeding up the search.

(4) Reeds-Shepp stepwise expansion

When expanding nodes, every interval l_{RS} connects the optimal node with the target node using Reeds-Shepp curve to generate Reeds-Shepp (RS) path. If the RS path is in a collision-free state, the node is not expanded, but the RS path is connected to the path previously obtained from the node expansion to form the final path. If the RS path is in a collision state, node expansion continues.

By using the Reeds-Shepp step-by-step expansion method. It effectively reduces the computational amount of node expansion and can improve the search speed, but the method is only suitable for use in regions with fewer obstacles and is not suitable for use in regions with dense obstacles. This is because most of the RS paths generated in regions with dense obstacles are in a collision state and need to be eliminated. Therefore too many generated RS paths will instead increase the search time.

II. D. 3) Reverse extension design in confined spaces

For the vertical and diagonal parking scenarios with narrow space, this paper makes the following improvements to the conventional Hybrid A★, by interchanging the start point and the target point of the parking path, so that the Hybrid A★ starts from the inside of the narrow space to the outside of the open space for the node expansion, in order to improve the efficiency of the autonomous parking path planning.

The specific workflow of the improved and obtained reverse expansion Hybrid A★ algorithm is shown in Figure 2, and its main steps are as follows:

(1) If the path target point is inside the narrow space, take the target point as the starting point of node expansion.

(2) Select the optimal node from the expanded alternative nodes according to the cost function, obtain the expansion step length by vehicle kinematics modeling at the optimal node, and expand a number of alternative nodes to form a search tree.

(3) Connect the optimal node with the target node by Reeds-Shepp step-by-step expansion method, if the connected path is in a collision-free state, the HybridA★ algorithm terminates, otherwise return to the previous step.

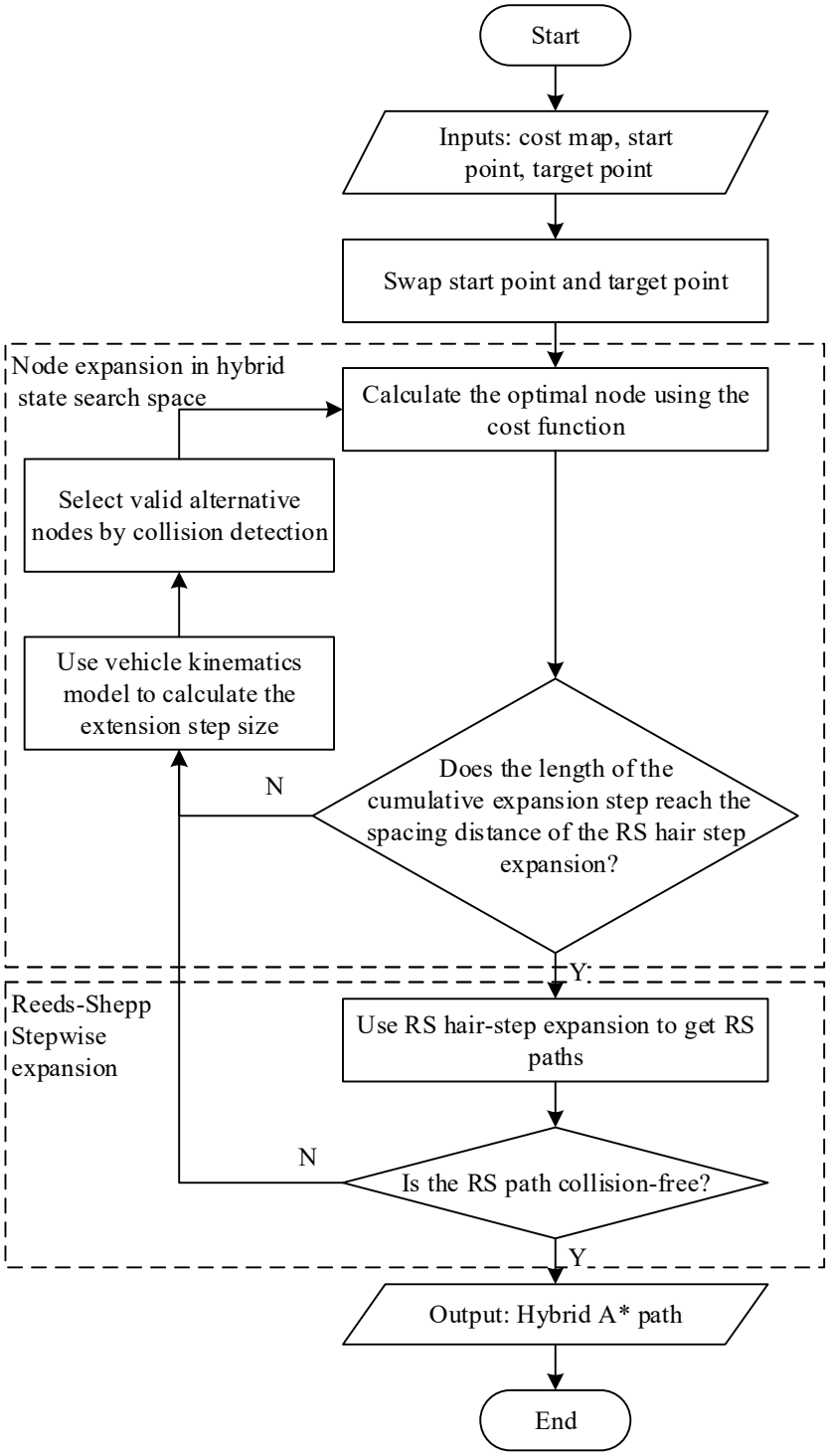

Figure 2: Reverse extension of the Hybrid A⋆ algorithm

III. Path planning simulation experiment for autonomous parking system

In this chapter, the proposed Hybrid A⋆ path planning algorithm is utilized for autonomous parking simulation experiments to verify the effectiveness of the algorithm.

III. A. Autonomous Parking Path Planning Simulation and Result Analysis

III. A. 1) Global path planning

In order to verify the feasibility of the reverse expansion Hybrid A* algorithm in global parking path planning, simulation experiments are conducted in this section. Taking the lower left corner of the map as the coordinate origin, a parking lot environment with a length of 80m and a width of 60m is built, and there are 5 rows of free parking spaces in the parking lot. The global path planning simulation is shown in Figure 3. The vehicle starts from the top-left corner of the map as the starting position and travels to the vicinity of the parking spaces, ready for further parking operations.

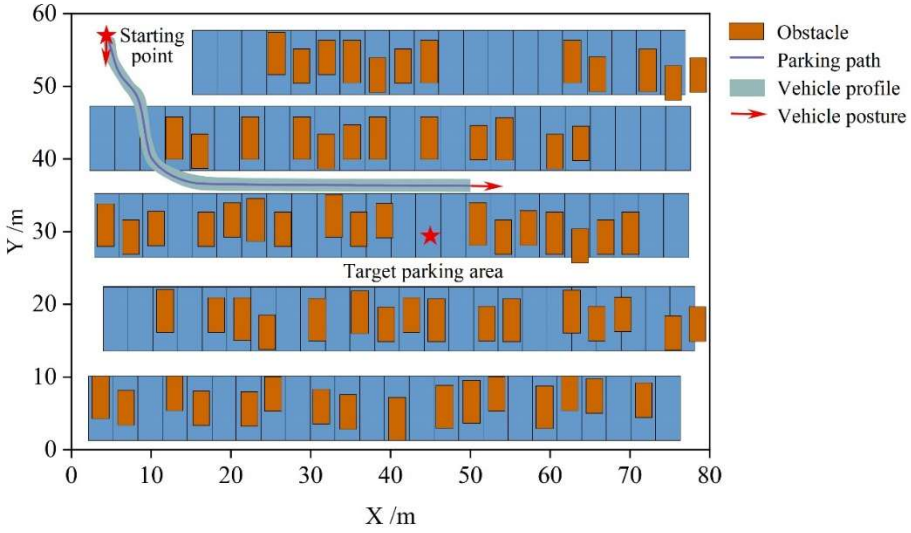

Figure 3: Simulation of global path planning

In the case of a more complex path, the vehicle can be combined with the Reeds-Shepp curve to consider the node expansion mode of the vehicle backward, and plan a compliant path under the vehicle kinematics constraints. Combined with the Reeds-Shepp curve of the backward expansion Hybrid A * global path planning simulation is shown in Figure 4, planning the vehicle from the starting point to the target end point, the vehicle in the middle of the path in the narrow position will be planned for the existence of switching the driving direction of the situation of the reciprocating path.

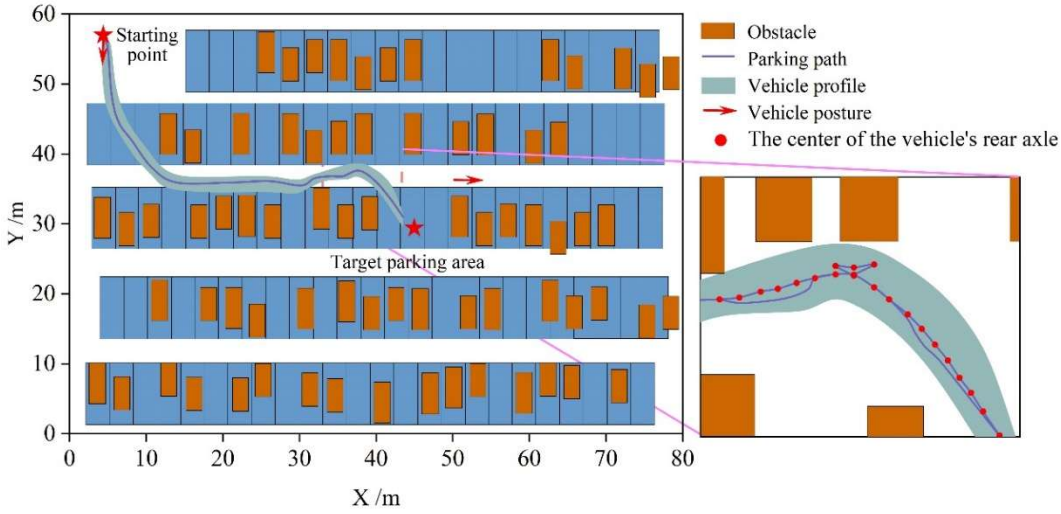

Figure 4: Reverse extension of Hybrid A* global path planning simulation

If the vehicle parking endpoints with different postures are set, the reverse expansion Hybrid A* algorithm will plan different parking driving paths, and the global path planning with different endpoint postures is simulated as shown in Fig. 5, and (a) and (b) denote the planning paths 1 and 2, respectively.

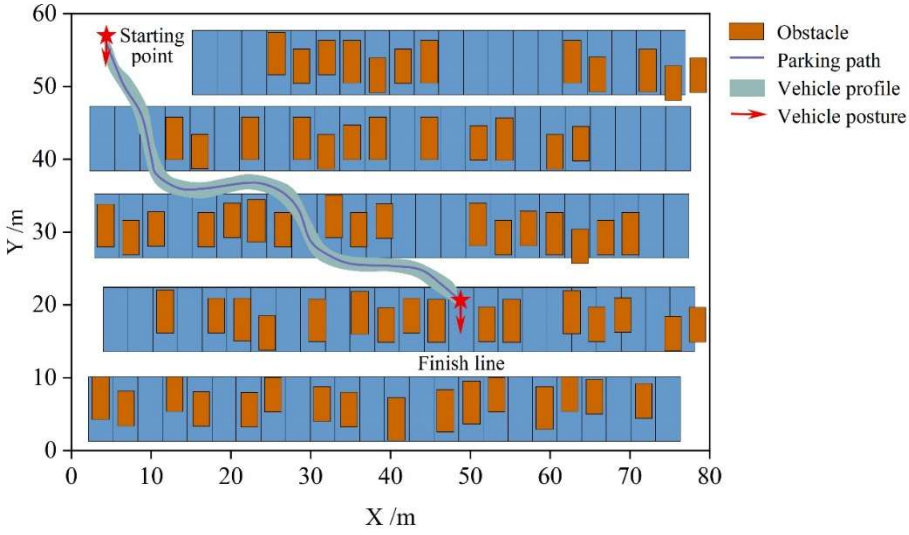

(a) Plan path 1

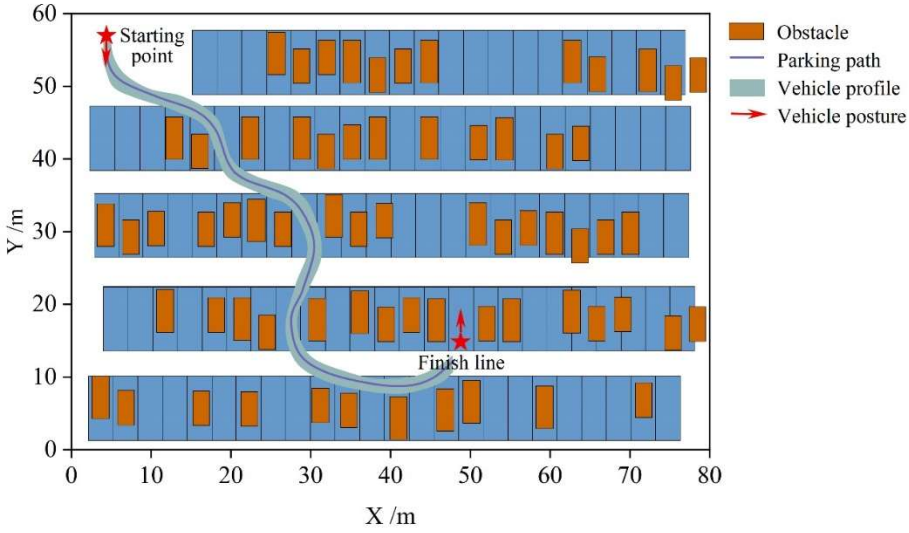

(b) Plan Path 2

Figure 5: Simulation of different endpoint poses for global path planning

The path planning times for the above four scenarios are shown in Table 1. The global path planning times are all within 1.4s, and the planning algorithm can plan the parking path completely and quickly.

Table 1: Path planning time

Plan the scene	Figure 3	Figure 4	Figure 5(a)	Figure 5(b)
Plan time /s	0.75	1.32	1.01	1.05

The weight of the cost function in the reverse expansion Hybrid A* algorithm has a large impact on the vertical parking path. In this paper, we analyze the cost function in the algorithm about the switch between steering and vehicle driving direction, and choose the short distance parking path near the parking space. The starting and ending positions of vehicle path planning in the three working conditions are the same, and the weights of the cost function are different. In Case 1, the cost of vehicle traveling direction switching is heavily weighted, and the path planning tends to exchange a larger reversing space for fewer times of vehicle traveling direction switching. In Case 2, the vehicle steering cost weight is small, and the path tends to obtain a shorter path with a larger steering angle. Combining the above planning features, the steering cost weight is increased and the vehicle traveling direction

switching cost weight is reduced in Case 3, and the obtained path planning results are more in line with the actual situation of parking, and the driving comfort is better.

III. A. 2) Parking Entry Path Planning

In order to verify the feasibility of the reverse expansion Hybrid A* algorithm in the parking space path planning, this paper builds a simulation of the parking lot environment, the parking lot is 80m long and 60m wide, which will be abstracted as 5 rows, 12 parking spaces per row.

Vertical parking entry simulation is shown in Figure 6, if you do not switch the direction of vehicle travel, in the case of the head of the vehicle into the parking space, the vehicle will plan a path away from the parking space first, which requires a larger parking space.

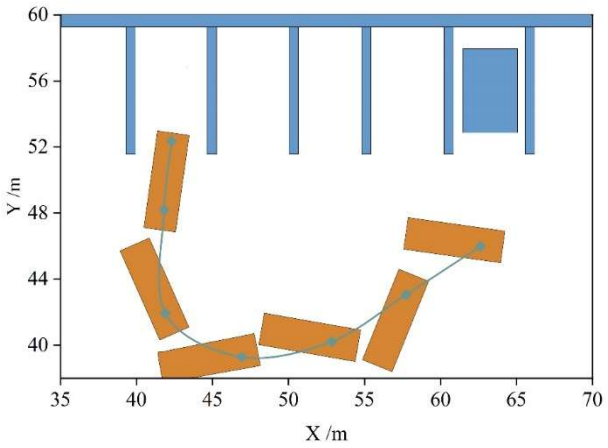

Figure 6: Vertical parking path planning

Vertical Spaces Reversing Parking As shown in Figure 7, the vehicle can be parked in a smaller parking space by switching the direction of travel.

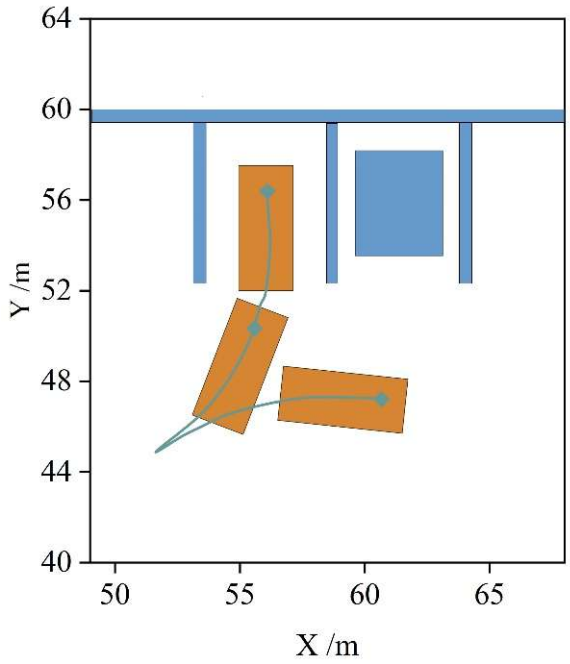

Figure 7: Vertical parking space reversing parking path planning

The parallel parking condition is shown in Fig. 8. After setting the parking space parameters and the starting point, the vehicle position attitude of the vehicle can be obtained at each moment during the parking process. The orange box indicates the vehicle body attitude when the vehicle is traveling according to the planned path, and its envelope

is the body coverage area. The vehicle is traveling according to the planning of two tangent arcs, the radius R_1 of the first arc is 16.18m and the radius R_2 of the second arc is 1.74m.

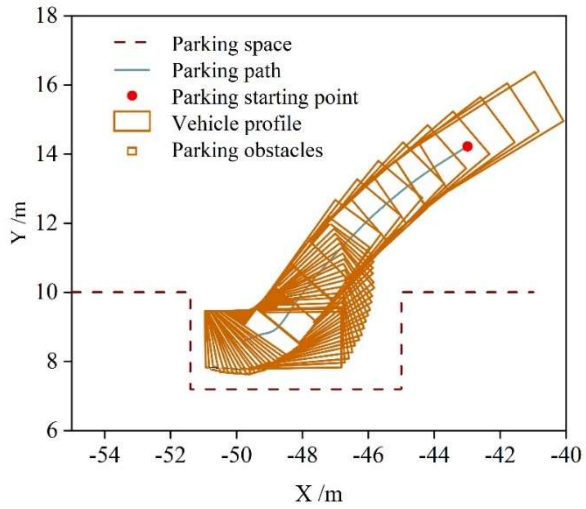

Figure 8: MATLAB simulation of parking path planning

Obstacles in the vicinity of the parking space can have an impact on the path planning results. The MATLAB simulation of the parking entry path planning for the case with obstacles is shown in Fig. 9, where the vertex coordinates of the parking space are kept constant and are represented by dashed lines in the figure. The vehicle length, vehicle width, and the distance between the front and rear overhangs of the vehicle are kept constant, the starting heading angle of the vehicle is 40 □, and the starting position of the vehicle is represented by a dark yellow hollow point. The center coordinates of the obstacle are represented as dark cyan dots with an expansion radius of 0.6 m. The trajectories of the two parking segments of the vehicle are represented as magenta and light blue lines, respectively, and the body attitude of the vehicle when it follows the planned path is represented as an orange box, and the radius of the first segment arc, R_1, is 68.49 m, and that of the second segment arc, R_2, is 2.48 m. The radius of the second segment arc is 2.48 m, and that of the second segment arc is 2.48 m. The vehicle's body position is indicated by the orange box. The radius of the two-segment planning arc is larger than when there is no obstacle.

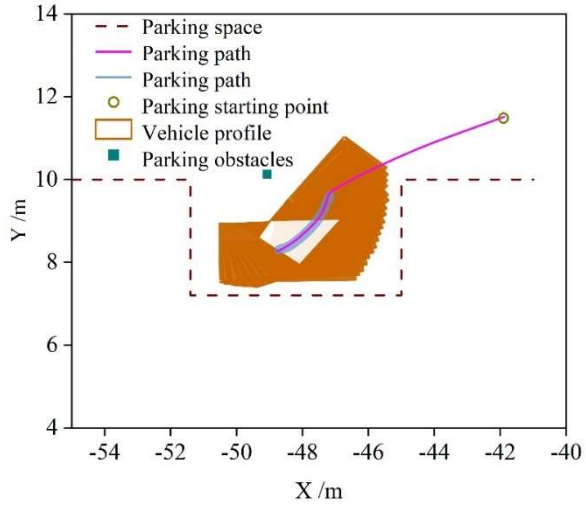

Figure 9: MATLAB simulation of parking path planning in the presence of obstacles

The actual length of the measurement of the position where the vehicle intersects with the parking space line is 12cm, and the width is 70cm. Considering that the position is located at the corner of the parking space, and the body has a certain curvature, there is a certain space between the vehicle and the edge of the parking space, so the error is within the acceptable range.

III. B. Parking Scenario Simulation Verification

In this section, simulation experiments of parking scenarios are carried out in terms of different parking space sizes and different parking speeds to further validate the effectiveness of the proposed reverse-expanded Hybrid A* algorithm.

III. B. 1) Simulation experiments with different parking space sizes

In this subsection, simulation experiments are conducted on two different sizes of parallel parking spaces to investigate the effect of different space dimensions on the gyratory curve parking method. The coordinates of the end position are (1.163,-0.975), the vertical coordinate of the start position is $y_0 = 2.1$, and the speed of the vehicle is constant at 3km/h. One of the parallel parking spaces has the dimensions of 7.2 meters in length and 2.6 meters in width, and the other one has the dimensions of 7.4 meters in length and 2.4 meters in width.

A comparison of the simulation results for the two parking sizes is shown in Fig. 10. Where (a) denotes the vehicle rear axle center point path, (b) denotes the vehicle parking path, (c) denotes the vehicle heading angle, and (d) the parking path curvature.

It can be seen that the planned paths under the two parking sizes overlap, and the coordinates of the parking start position are both (8.564,2.100), and the vehicle paths are also the same, with only the orange rectangular contour appearing, which indicates that the paths under the two parking sizes not only have the same transverse and vertical coordinates, but also the vehicle's body angle is identical, which can be verified from Fig. 10(c), and the vehicle heading angle obtained by both sizes of the The curves of vehicle heading angle with transverse coordinates also overlap, and the maximum heading angle is 0.812 rad for both of them, and the curvature of the paths is also the same for both of them in Fig. 10(d). Therefore, it can be concluded that when the size of the parking space meets the requirement of the minimum parking space, the end position of the parking is fixed and the longitudinal coordinates of the starting position and the speed of the vehicle are the same, the increase in the size of the parking space has no effect on the parking path generated by the vehicle planning. However, as the increase of the length of the parking space will make the vehicle farther away from the upper apex of the outer side of the parking space during the parking process, the vehicle will be safer. Whereas, the increase in the width of the parking space has no significant improvement on the safety improvement of the parking.

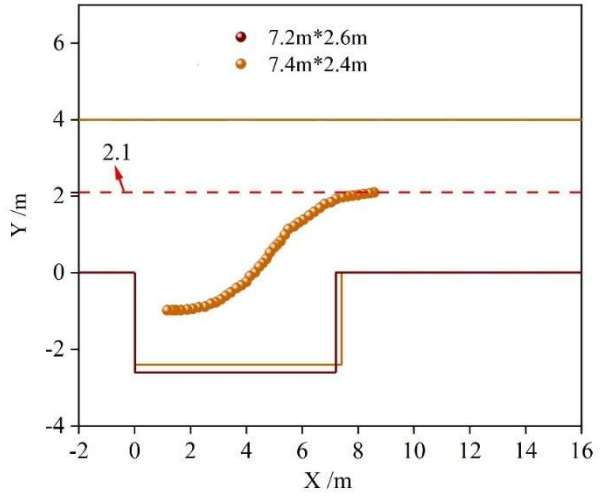

(a) The path of the center point of the vehicle's rear axle

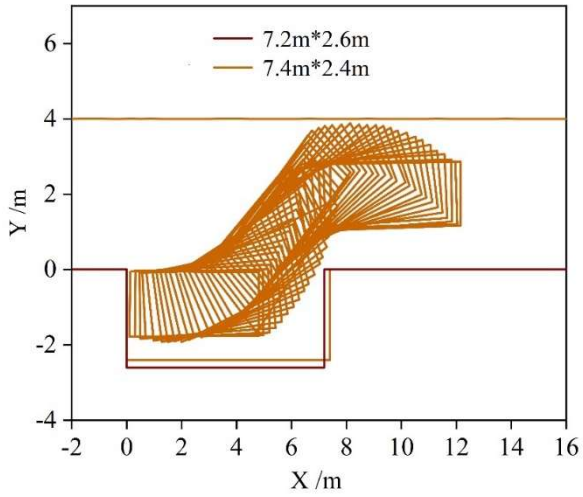

(b) Vehicle parking paths

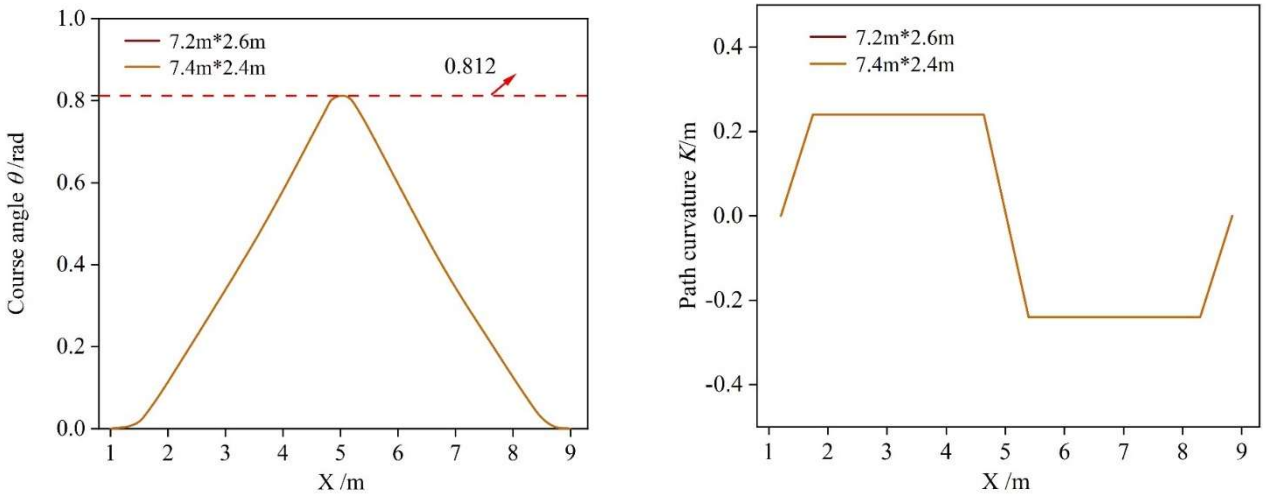

(c) Vehicle heading angle (d) Curvature of parking path

Figure 10 Simulation results of two parking space sizes

III. B. 2) Simulation experiments with different parking speeds

This subsection investigates the effect of different parking speeds on the gyratory curve parking planning path by conducting simulation experiments at two vehicle speeds. The dimension of the parallel parking space is 7.4 meters long and 2.4 meters wide. The coordinates of the end position are (1.163,-0.975), the longitudinal coordinate of the start position is $y_0 = 1.6$, and the vehicle speeds are constant at 3km/h and 6km/h respectively.

A comparison of the parking simulation results for two different vehicle speed conditions is shown in Fig. 11. Where (a) represents the vehicle rear axle center point path, (b) represents the vehicle parking path, (c) represents the vehicle heading angle, and (d) the parking path curvature. The burgundy curve indicates the vehicle speed of 3km/h working condition, while the orange curve indicates the vehicle speed of 6km/h working condition.

From Fig. 11(a), it can be seen that there are differences in the planned paths under the conditions that the two vehicle speeds have the same end position and the same longitudinal coordinates of the start position, and the most obvious difference is that the horizontal coordinates of the start position of the two conditions are different, with the coordinates of the start position of the v=6km/h condition being (8.680,1.600) and that of the v=3km/h condition being (8.112,1.600), which indicates that the v=6km/h condition is the most important condition for parking path curvature. This indicates that the aisle length required for v=6km/h condition is longer.

From Fig. 11(b), it can be seen that when using the reverse expansion Hybrid A★ algorithm for gyratory curve parking planning, the vehicle is safely parked into the designated position of the parking space under both speed conditions, and the orange rectangular contour indicates that the vehicle's body change is relatively larger for the v=3km/h condition.

Figure 11(c) shows the simulation results of the vehicle heading angle variation with the horizontal axis for the two conditions, both of which are shown in the shape of an approximate bell-shaped curve, with the middle part of the burgundy curve being higher and narrower, and the middle of the orange curve being lower and wider, and the blue-burgundy curve having a maximum heading angle of 0.722 rad at the corresponding coordinates (4.706,0.326), and the orange curve having a maximum heading angle of 0.722 rad at coordinates (5.009,0.326), and the blue-burgundy curve having a maximum heading angle of 0.722 rad at coordinates (5.009,0.326).) has a maximum heading angle of 0.686 rad. In terms of the parking path reversal process, from the same parking end position, the coordinates of the two conditions to reach the maximum heading angle can be seen that both have the same vertical coordinates, while the horizontal coordinates of the v=3km/h condition are smaller, i.e., the vehicle is more rearward, and the maximum heading angle is relatively larger, then the direction of the vehicle body is more upward, which is different from Fig. 11(a) and (b) which show that the that the path is more rearward and upward is consistent.

In Fig. 11(d), from the parking end position, the path curvature changes faster for the *v*=3km/h condition, reaching the maximum path curvature corresponding to a transverse distance of 0.54 meters, while the transverse distance for the *v*=6km/h condition is 1.02 meters. Whereas this section of curvature corresponds to the gyratory curve phase, it is shown that the increase in speed leads to an increase in the arc length of the gyratory curve section. The *v*=3km/h case not only reaches the maximum curvature faster than the *v*=6km/h case, but also has a longer lateral distance in the maximum curvature stage, then it means that the *v*=3km/h case turns over a larger angle in the circular curve stage, which is reflected in the relatively larger maximum heading angle corresponding to Fig. 11(c).

The simulation data calculation results show that the minimum parking space size of v=6km/h is 7.058m×2.205m, while the minimum parking space size of v=3km/h is 6.821m×2.164m, and v=6km/h is relative to v=3km/ The length of the parking space is increased by 0.207m and the width of the parking space is increased by 0.041m.

Therefore, the required minimum space size is different under different parking speeds, and the larger the speed, the larger the required space size. As the parking planning is in the low-speed condition, the minimum required parking space size of the gyratory curve increases only slightly under the limited speed increase, and the actual parking space size can fully satisfy the planning conditions of the algorithm.

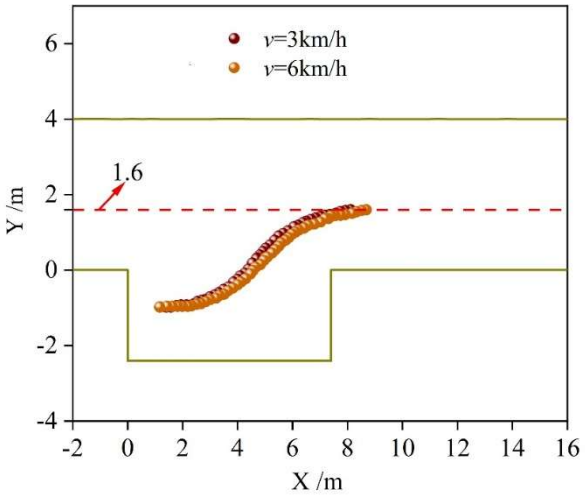

(a) The path of the center point of the vehicle's rear axle

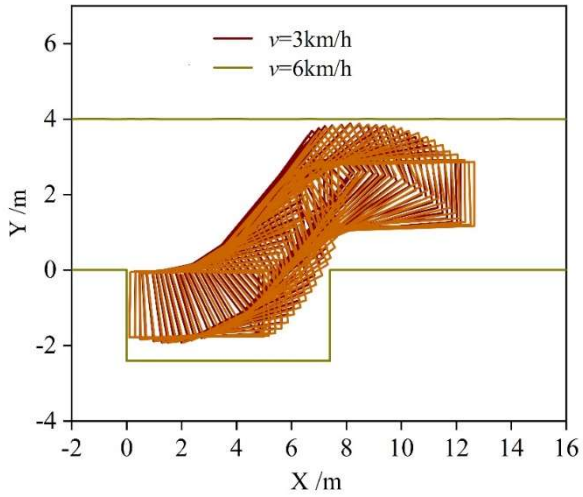

(b) Vehicle parking paths

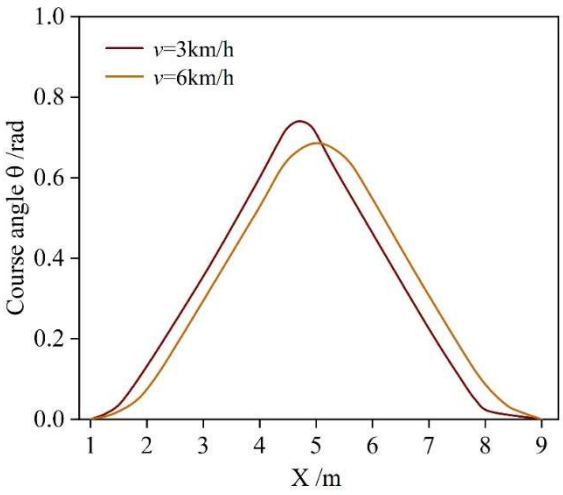

(c) Vehicle heading angle

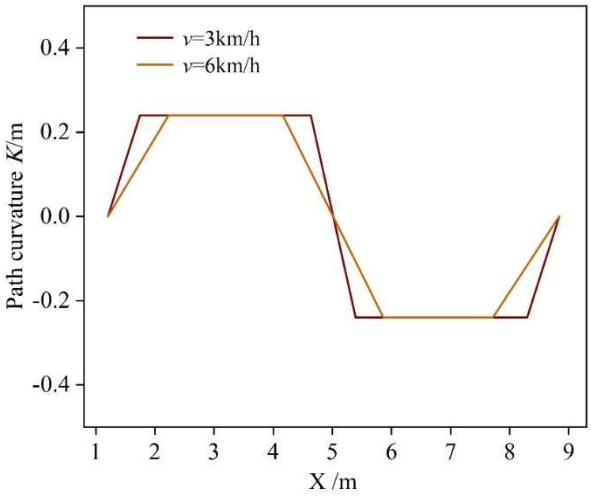

(d) Curvature of parking path

Figure 11: Simulation results of different parking speeds

IV. Conclusion

In this study, the combination of multi-sensor fusion localization and improved Hybrid A* path planning algorithm provides an effective technical solution for autonomous parking in closed residential areas. An environment sensing system constructed by integrating 12 ultrasonic sensors and 4 high-definition cameras achieves accurate modeling of the complex parking environment. The establishment of camera projection model, IMU measurement model and wheel tachometer kinematic model lays a theoretical foundation for multi-source data fusion, which significantly improves the system's localization accuracy and environment adaptation capability.

The introduction of the inverse expansion strategy significantly improves the search efficiency of the Hybrid A* algorithm in a narrow space. Experimental results show that the path planning time of the algorithm in the complex parking lot scene is controlled within 1.32s, which meets the real-time demand. The test of different parking speeds

shows that the arc length of the first gyratory curve is 1.02 meters when the vehicle speed is 6km/h, which is significantly longer than the 0.54 meters in the 3km/h condition, verifying the influence law of speed on path planning.

The inflated collision detection algorithm ensures parking safety, and achieves centimeter-level collision prediction accuracy through the accurate modeling of rectangular vehicle model. The optimized design of the cost function effectively balances multiple factors such as path length, steering frequency and driving direction switching, making the planning path smoother and more natural. The algorithm shows good robustness in various scenarios, such as vertical parking and parallel parking, which provides important technical support for the engineering application of autonomous parking system for intelligent networked vehicles in complex environments in residential areas, and has a broad practical prospect.

Funding

This research was supported by the Science and Technology Research Program of Chongqing Municipal Education Commission (Grant No. KJQN202303223).

References

[1] Vařbuchta, P., & Hromádka, V. (2023). Index of Residential Development: Evaluation of the Possibility of New Residential Construction Depending on the City Plan. Buildings, 13(12), 3016.
[2] Buttimer, A. (2015). Social space and the planning of residential areas. In The human experience of space and place (pp. 21-54). Routledge.
[3] Wen, Z., Zhang, S., Yang, Y., Zheng, X., Song, Z., Zhou, Y., & Hao, J. (2023). How does enclosed private residential green space impact accessibility equity in urban regions? A case study in Shenzhen, China. Urban Forestry & Urban Greening, 85, 127968.
[4] Cihan, M. M., & Erdönmez Dinçer, M. E. (2018). An Examination of the Relationship Between Enclosed Residential Areas, Other Residences, and Public Spaces. MEGARON/YILDIZ TECHNICAL UNIVERSITY, FACULTY OF ARCHITECTURE E-JOURNAL, 13(1), 102-116.
[5] Gao, X., Million, A., & Wang, R. (2023). Gating and gatedness: interpreting the procedural refiguration of an enclosed residential compound in Guangzhou. Technische Universität Berlin.
[6] Yan, T., Jin, H., & Zhao, H. (2019). The relationship between the form of enclosed residential areas and microclimate in severe cold area of China. In Sustainability in Energy and Buildings: Proceedings of SEB 2019 (pp. 135-146). Singapore: Springer Singapore.
[7] Li, Y., Chen, Q., Cheng, Q., Li, K., Cao, B., & Huang, Y. (2022). Evaluating the influence of different layouts of residential buildings on the urban thermal environment. Sustainability, 14(16), 10227.
[8] Tan, T. H. (2016). Residential satisfaction in gated communities: Case study of desa park city, Kuala Lumpur, Malaysia. Property Management, 34(2), 84-99.
[9] Li, M., & Xie, J. (2023). Social and spatial governance: the history of enclosed neighborhoods in urban China. Journal of Urban History, 49(4), 723-744.
[10] Ashrafi, K., Motlagh, M. S. P., Mousavi, M. S., Niksokhan, M. H., & Vosoughifar, H. R. (2017). An experimental and numerical investigation of velocity in an enclosed residential complex parking area. Heat and Mass Transfer, 53(2), 451-463.
[11] Gabbe, C. J., Pierce, G., & Clowers, G. (2020). Parking policy: The effects of residential minimum parking requirements in Seattle. Land Use Policy, 91, 104053.
[12] De Gruyter, C., Davies, L., & Truong, L. T. (2021). Examining spatial variations in minimum residential parking requirements in Melbourne. Journal of Transport Geography, 94, 103096.
[13] Duvanova, I., Simankina, T., Shevchenko, A., Musorina, T., & Yufereva, A. (2016). Optimize the use of a parking space in a residential area. Procedia Engineering, 165, 1784-1793.
[14] Dibaei, M., Zheng, X., Jiang, K., Abbas, R., Liu, S., Zhang, Y., ... & Yu, S. (2020). Attacks and defences on intelligent connected vehicles: A survey. Digital Communications and Networks, 6(4), 399-421.
[15] Wang, B., Han, Y., Wang, S., Tian, D., Cai, M., Liu, M., & Wang, L. (2022). A review of intelligent connected vehicle cooperative driving development. Mathematics, 10(19), 3635.
[16] Liu, Y., & Fang, X. (2016). Big wave of the intelligent connected vehicles. China Communications, 13(2), 27-41.
[17] Lee, J., Huang, H., Wang, J., & Quddus, M. (2022). Road safety under the environment of intelligent connected vehicles. Accident Analysis & Prevention, 170, 106645.
[18] Mladenović, M., Delot, T., Laporte, G., & Wilbaut, C. (2020). The parking allocation problem for connected vehicles. Journal of Heuristics, 26, 377-399.
[19] Channamallu, S. S., Kermanshachi, S., Rosenberger, J. M., & Pamidimukkala, A. (2023). A review of smart parking systems. Transportation Research Procedia, 73, 289-296.
[20] Chan, T. K., & Chin, C. S. (2021). Review of autonomous intelligent vehicles for urban driving and parking. Electronics, 10(9), 1021.
[21] Sayarshad, H. (2023). Designing intelligent public parking locations for autonomous vehicles. Expert Systems with Applications, 222, 119810.
[22] Li, C., Wang, S., Li, X., Zhao, F., & Yu, R. (2020). Distributed perception and model inference with intelligent connected vehicles in smart cities. Ad Hoc Networks, 103, 102152.
[23] Hongbo, G., Guotao, X., Xinyu, Z., & Bo, C. (2017). Autonomous parking control for intelligent vehicles based on a novel algorithm. The Journal of China Universities of Posts and Telecommunications, 24(4), 51-56.
[24] Paidi, V., Fleyeh, H., Håkansson, J., & Nyberg, R. G. (2018). Smart parking sensors, technologies and applications for open parking lots: a review. IET Intelligent Transport Systems, 12(8), 735-741.
[25] Kim Dongchan & Huh Kunsoo. (2023). Neural Motion Planning for Autonomous Parking. International Journal of Control, Automation and Systems,21(4),1309-1318.